Evaluation of the fourth-order tesseroid formula and new combination approach to precisely determine gravitational potential

WEN-BIN SHEN[1,2] AND XIAO-LE DENG[1]

1 School of Geodesy and Geomatics, Wuhan University, Luoyu Road 129, 430079 Wuhan, HuBei, China (wbshen@sgg.whu.edu.cn)

2 State Key Laboratory of Information Engineering in Surveying, Mapping and Remote Sensing, Wuhan University, 430079 Wuhan, China

Received: January 7, 2016; Revised: March 19, 2016; Accepted: April 4, 2016

ABSTRACT

Calculating topographic gravitational potential (GP) is a time-consuming process in terms of efficiency. Prism, mass-point, mass-line, and tesseroid formulas are generally used to calculate the topographic GP effect. In this study, we reformulate the higher-order formula of the tesseroid by Taylor series expansion and then evaluate the fourth-order formula by numerical tests. Different simulation computations show that the fourth-order formula is reliable. Using the conventional approach in numerical calculations, the approximation errors in the areas of the north and south poles are extremely large. Thus, in this study we propose an approach combining the precise numerical formula and tesseroid formulas, which can satisfactorily solve the calculation problem when the computation point is located in the polar areas or areas very near the surface. Furthermore, we suggest a "best matching choice" of new combination approach to calculate the GP precisely by conducting various experiments. Given the computation point at different positions, we may use different strategies. In the low latitude, we use a precise numerical formula, the fourth-order tesseroid formula, the second-order tesseroid formula, and the zero-order formula, in the 1° range (from the computation point), 1° to 15° range, 15° to 40° range, and the range outside 40°, respectively. The accuracy can reach $2 \times 10^{-5}\ m^2\ s^{-2}$. *For the high latitude, we use the precise numerical formula, fourth-order tesseroid, second-order tesseroid, and zero-order tesseroid formulas in the ranges of 0° to 1°, 1° to 10°, 10° to 30°, and the zones outside 30°, respectively. However, if an accuracy level of* $2 \times 10^{-5}\ m^2\ s^{-2}$ *is required, the zero-order tesseroid formulas should not be used and the second-order tesseroid formula should be used in the region outside 15° for the low latitude and in the region outside 10° for the high latitude.*

Keywords: Newton's integral, gravitational potential, tesseroid, new combination method

1. INTRODUCTION

Many researchers (*Forsberg, 1984*; *Kiamehr and Sjöberg, 2005*; *Kiamehr, 2006*; *Hirt et al., 2010*; *Sjöberg and Bagherbandi, 2011*; *Jena et al., 2012*; *Tenzer et al., 2012*; *Hirt et al., 2013*; *Chaves and Ussami, 2013*; *Claessens and Hirt, 2013*; *Majumdar and Bhattacharyya, 2014*; *Rexer and Hirt, 2014*) discussed the problems of precisely calculating the gravity effect (gravity anomaly, gravitational potential, gravity vector, gravity gradient, and so on) caused by terrain effects in recent decades. In these studies, various topography models are used, such as Earth2014 global topography model (*Hirt and Rexer, 2015*), SRTM digital elevation data (*Jarvis et al., 2008*), based on constant (e.g., 2.67 g cm^{-3}), CRUST2.0 (*Bassin et al., 2000*), CRUST1.0 (*Laske et al., 2013*), or GEMMA (*Reguzzoni and Sampietro, 2015*) density distributions. Determining the topographic effect in computing the gravitational potential (GP) plays a key role in establishing high-resolution and high-accuracy global/local gravity fields and geoids.

In recent decades, different studies compute the GP using various methods, which can be divided into two main kinds of approaches - the spatial domain forward modeling and spectral domain forward modeling (*Hirt and Kuhn, 2014*). In this paper, the spatial domain forward modeling is extensively discussed, which includes line-mass approach (*Tsoulis, 1999*; *Wild-Pfeiffer, 2008*), point-mass approach (*Tsoulis, 1999*; *Heck and Seitz, 2007*; *Wild-Pfeiffer, 2008*), layer-mass approach (*Tsoulis, 1999*; *Wild-Pfeiffer, 2008*), Gauss-Legendre cubature model (*Asgharzadeh et al., 2007*; *Wild-Pfeiffer, 2008*), polyhedral body model (*Tsoulis, 2012*; *D'Urso, 2013, 2014*), prism model (*Smith, 2000*; *Nagy et al., 2000, 2002*; *Han and Shen, 2010*; *D'Urso, 2012*), tesseroid model (*Anderson, 1976*; *Heck and Seitz, 2007*; *Grombein et al., 2013*; *Hirt and Kuhn, 2014*), or prism and tesseroid combination (*Tsoulis et al., 2009*; *Shen and Han, 2013, 2014, 2016*). The prism and tesseroid formulas, and their combination method, are the most widely applied ones among these approaches.

The prism method (*Forsberg, 1984*; *Nagy et al., 2000, 2002*) for calculating the GP is widely used in local gravity field/geoid modeling (*Han and Shen, 2010*; *D'Urso, 2012*). Although this method has a rigorously closed expression and can be solved analytically, it needs ways to correct for Earth curvature by lowering prisms in some distance and by changing their orientation (see *Forsberg, 1984*, for more details) because the surface of the Earth is nearly spherical. Similar to the tesseroid method, the computation time largely increases when the prism method is used and the terrain is divided into finer grids.

A tesseroid, which was first introduced by *Anderson (1976)*, is defined as a body with boundaries that constitute a pair of ellipsoidal height, meridional planes, and coaxial circular cones (see Fig. 1), and has been discussed in detail by *Heck and Seitz (2007)*. The tesseroid method for modeling the topography GP effect was applied by many researchers (*Tsoulis et al., 2009*) because of its numerous advantages over other methods.

The combination of the prism and second-order tesseroid model was also extensively used in the local area (*Tsoulis et al., 2009*; *Shen and Han, 2013*) or global geoid determination (*Shen and Han, 2014, 2016*). Its advantage over the two separate methods is that it considers both proper high calculation accuracy and efficiency.

Scholars still use the second-order tesseroid formula based on the Taylor series expansion, which was proposed by *Heck and Seitz (2007)*, and then used by various

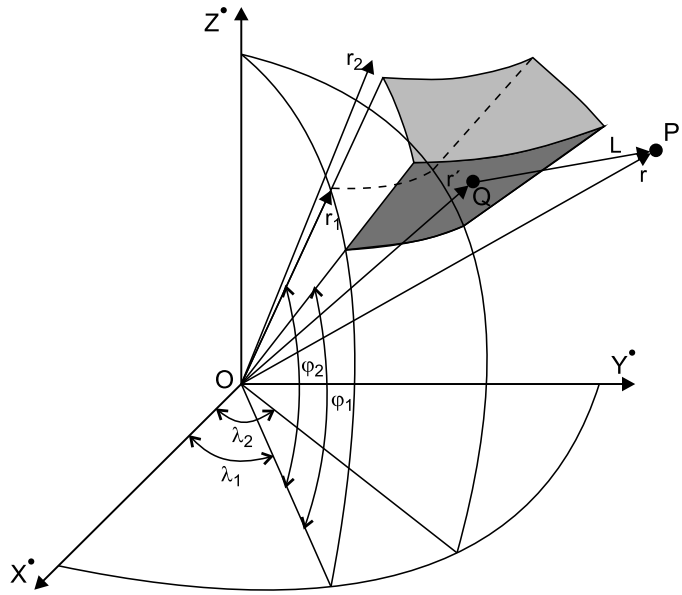

Fig. 1. The geometry of the tesseroid in global geocentric spherical coordinates (redrawn after *Kuhn, 2003*).

authors (*Tsoulis et al., 2009*; *Chaves and Ussami, 2013*; *Claessens and Hirt, 2013*; *Grombein et al., 2013*; *Shen and Han, 2013, 2016*; *Hirt and Kuhn, 2014*) However, compared with the ultra-high resolution of the topography model (Earth2014, SRTM, GTOPO30, and others) and successive higher accuracy requirement, the second-order tesseroid formula (based on the Taylor series expansion) is insufficient at the very vicinity of the computation point. Thus, formulating a fourth-order or even higher-order tesseroid formula for high-accuracy calculation especially for the mass-elements in the very vicinity of the computation point is necessary.

When the formula is applied in reality of the global related potential application, many factors should be considered, such as the flattening of the Earth, the geometry of the mass source and mass density distribution etc. In this paper we just simplify these issues to focus on tests of the fourth-order tesseroid formula and comparison of the conventional combination method and new combination method proposed here.

In this study, extending the work of *Heck and Seitz (2007)*, we provide the fourth-order tesseroid formula based on the Taylor series expansion of the Newton's integral. The tesseroid method for modeling the GP is surveyed in Section 2, and the series expansion of *Heck and Seitz (2007)* is also provided therein. We note that the general Taylor series expansion given by *Heck and Seitz (2007)* as well as that formula cited by *Grombein et al. (2013)* from which the gravitational attraction of a tesseroid is derived, is incorrect; however the second-order formula is correct, as it was pointed out by *Deng et al. (2016)*. A correct general Taylor series expansion expression of tesseroid formula is provided in Section 2. We use a uniform spherical mass shell model to conduct numerical

tests based on different-order tesseroid formulas, calculate the GP, and compare the results based on different arrangements of the computation point presented in Section 3. Section 4 shows the errors in the north and south polar areas are quite large by the numerical tests. Hence we solve the pole and very near-zone problems using the new combination method. Section 5 discusses the relevant problems and concludes this paper. Appendix A lists the coefficients of the zero-order, second-order and fourth-order tesseroid formulas.

2. FORMULAS FOR GRAVITATIONAL POTENTIAL GENERATED BY A TESSEROID

The gravitational potential V generated by an element unit tesseroid with a constant mass-density ρ can be expressed by Newton's integral (*Heck and Seitz, 2007*):

$$V(r,\varphi,\lambda) = G\rho \int_{\lambda_1}^{\lambda_2}\int_{\varphi_1}^{\varphi_2}\int_{r_1}^{r_2} \frac{r'^2\cos\varphi'}{l}\, dr'\, d\varphi'\, d\lambda' \ , \tag{1}$$

$$l = \sqrt{r^2 + r'^2 - 2rr'\cos\psi} \ , \tag{2}$$

$$\cos\psi = \sin\varphi\sin\varphi' + \cos\varphi\cos\varphi'\cos(\lambda' - \lambda) \ , \tag{3}$$

where G is the Newtonian gravitational constant, r, φ, λ are the spherical coordinates of the computation point P, r', φ', λ' are the spherical coordinates of the running integration point Q, l is the Euclidean distance between points P and Q, and ψ denotes the angle between the position vectors of points P and Q as the spherical distance.

Given that Eq. (1) cannot be analytically solved by integration, *Heck and Seitz (2007)* used the Taylor series expansion method to solve this equation.

The geometrical center point $Q_0(r_0, \varphi_0, \lambda_0)$ of the tesseroid can be set as follows (*Heck and Seitz, 2007*; *Grombein et al., 2013*):

$$r_0 = \frac{r_1 + r_2}{2} \ , \quad \varphi_0 = \frac{\varphi_1 + \varphi_2}{2} \ , \quad \lambda_0 = \frac{\lambda_1 + \lambda_2}{2} \ . \tag{4}$$

Thus, the Taylor expansion at $Q_0(r_0, \varphi_0, \lambda_0)$ of the integral kernel $\left(r'^2\cos\varphi'\right)/l$ in Eq. (1) can be expressed as follows:

$$K(r',\varphi',\lambda') = \frac{r'^2\cos\varphi'}{l} = \sum_{i,j,k} K_{ijk}\frac{1}{i!\,j!\,k!}(r'-r_0)^i(\varphi'-\varphi_0)^j(\lambda'-\lambda_0)^k \ , \tag{5}$$

where

$$K_{ijk} = \left.\frac{\partial^{i+j+k}K(r',\varphi',\lambda')}{\partial r'^i\,\partial\varphi'^j\,\partial\lambda'^k}\right|_{r'=r_0,\,\varphi'=\varphi_0,\,\lambda'=\lambda_0} \ , \tag{6}$$

$$K\left(r_0, \varphi_0, \lambda_0\right) = \frac{r_0^2 \cos\varphi_0}{l_0} \ . \tag{7}$$

We note that, in *Heck and Seitz (2007)* as well as *Grombein et al. (2013)*, the kernel function $K\left(r', \varphi', \lambda'\right) = \left(r'^2 \cos\varphi'\right) \Big/ l$ is expressed as follows:

$$K\left(r', \varphi', \lambda'\right)_{HS} = \frac{r'^2 \cos\varphi'}{l} = \sum_{i,j,k} K_{ijk} \frac{1}{\left(i+j+k\right)!} \left(r'-r_0\right)^i \left(\varphi'-\varphi_0\right)^j \left(\lambda'-\lambda_0\right)^k \ . \tag{8}$$

However, the correct expression should be written as Eq. (5) rather than Eq. (8). In particular, the factor $1/\left(i+j+k\right)!$ that appears in Eqs (10), (23) and (33) of *Heck and Seitz (2007)* and Eq. (31) of *Grombein et al. (2013)* should be correctly written as factor $1/\left(i!\,j!\,k!\right)$. Fortunately, various international authors (e.g., *Wild-Pfeiffer, 2008*; *Tsoulis et al., 2009*; *Chaves and Ussami, 2013*; *Shen and Han, 2013*; *Du et al., 2015*) quoted only the second-order expression given by *Heck and Seitz (2007)*, which is correct because of the occasional coincidence of $1/\left(i+j+k\right)! = 1/\left(i!\,j!\,k!\right)$, due to the fact that $i + j + \mathrm{k} = 2$; $i, j, k = 0, 2$ (e.g., $1/\left(2+0+0\right)! = 1/\left(2!0!0!\right) = 1/2$) (*Deng et al., 2016*).

By inserting Eq. (5) into Eq. (1), we derive the following expression:

$$\begin{aligned} &V\left(r, \varphi, \lambda\right) \\ &= G\rho \int_{\lambda_1}^{\lambda_2} \int_{\varphi_1}^{\varphi_2} \int_{r_1}^{r_2} \sum_{i,j,k} K_{ijk} \frac{1}{i!\,j!\,k!} \left(r'-r_0\right)^i \left(\varphi'-\varphi_0\right)^j \left(\lambda'-\lambda_0\right)^k \, dr' \, d\varphi' \, d\lambda' \ , \end{aligned} \tag{9}$$

which can be successively integrated. For instance, the following equation can be derived out (*Heck and Seitz 2007*):

$$\int_{\lambda_1}^{\lambda_2} \left(\lambda'-\lambda_0\right)^i \, d\lambda' = \int_{-\Delta\lambda/2}^{\Delta\lambda/2} \left(\lambda''\right)^i \, d\lambda'' = \frac{1+\left(-1\right)^i}{\left(i+1\right)2^{i+1}} \left(\Delta\lambda\right)^{i+1} = \begin{cases} 0 \ , & i \text{ is odd} \ , \\ \dfrac{\left(\Delta\lambda\right)^{i+1}}{\left(i+1\right)2^i} \ , & i \text{ is even} \ , \end{cases} \tag{10}$$

where

$$\Delta r = r_2 - r_1 \ , \quad \Delta\varphi = \varphi_2 - \varphi_1 \ , \quad \Delta\lambda = \lambda_2 - \lambda_1 \tag{11}$$

are the three coordinate differences of the tesseroid (or dimensions of the tesseroid).

By combining Eqs (9)–(11), we can obtain the final GP Taylor series expansion of the tesseroid as follows:

$$V\left(r, \varphi, \lambda\right) = G\rho \sum_{i,j,k} K_{ijk} \frac{1}{i!\,j!\,k!} \frac{\left(\Delta r\right)^{i+1}}{2^i \left(i+1\right)} \frac{\left(\Delta\varphi\right)^{j+1}}{2^j \left(j+1\right)} \frac{\left(\Delta\lambda\right)^{k+1}}{2^k \left(k+1\right)} \ , \tag{12}$$

where i, j, and k are even integer numbers (i.e., $i, j, k = 0, 2, 4, 6, \ldots$), and the coefficient K_{ijk} is defined by Eq. (6).

Using Eq. (12), we can obtain any order Taylor series expansion. For instance, the expressions of the zero-order, second-order, and fourth-order Taylor series expansions can be written as follows:

$$V_0 = G\rho\,\Delta r\Delta\varphi\Delta\lambda\left(K_{000} + \mathcal{O}\left(\Delta^2\right)\right), \tag{13}$$

$$V_2 = G\rho\,\Delta r\Delta\varphi\Delta\lambda\left[K_{000} + \frac{1}{24}\left(K_{200}\Delta r^2 + K_{020}\Delta\varphi^2 + K_{002}\Delta\lambda^2\right) + \mathcal{O}\left(\Delta^4\right)\right], \tag{14}$$

$$\begin{aligned} V_4 = G\rho\,\Delta r\Delta\varphi\Delta\lambda\Bigg[& K_{000} + \frac{1}{24}\left(K_{200}\Delta r^2 + K_{020}\Delta\varphi^2 + K_{002}\Delta\lambda^2\right) \\ & + \frac{1}{576}\left(K_{220}\Delta r^2\Delta\varphi^2 + K_{202}\Delta r^2\Delta\lambda^2 + K_{022}\Delta\varphi^2\Delta\lambda^2\right) \\ & + \frac{1}{1920}\left(K_{400}\Delta r^4 + K_{040}\Delta\varphi^4 + K_{004}\Delta\lambda^4\right) + \mathcal{O}\left(\Delta^6\right)\Bigg], \end{aligned} \tag{15}$$

where the Landau symbols $\mathcal{O}\left(\Delta^2\right)$, $\mathcal{O}\left(\Delta^4\right)$, $\mathcal{O}\left(\Delta^6\right)$ indicate respectively the neglected terms of the second and higher order terms of the combination of the small quantities Δr, $\Delta\varphi$, $\Delta\lambda$.

We note that despite of the error in general expression of *Heck and Seitz (2007)* and *Grombein et al. (2013)*, the second-order approximation given therein is correct because of occasional coincidence, as mentioned earlier (for details see also *Deng et al., 2016*).

The expressions of the zero-order coefficient K_{000}, second-order coefficients K_{200}, K_{020}, K_{002}, and fourth-order coefficients K_{220}, K_{202}, K_{022}, K_{400}, K_{040}, K_{004} are listed in Appendix A.

3. NUMERICAL TESTS FOR FORMULAS

Here we perform numerical tests to evaluate the accuracy of Eqs (13)–(15), which also confirm the validity of Eq. (12). We compare the time cost of computation, precision, and error differences among the results of the calculated GPs based on different scenarios. And all of the simulative calculations are based on the spherical approximation, which neglect the flattening of the Earth.

We calculate the GP value of a uniform homogeneous spherical shell for comparison. The GP V_{true} at the computation point P on and outside the spherical shell can be accurately calculated (*Heiskanen and Moritz, 1967*; *Vaníček et al., 2001*; *Karcol, 2011*) as follows:

$$V_{\text{true}} = \frac{4}{3}\pi G\rho\frac{R^3 - R_1^3}{r}, \tag{16}$$

where R and R_1 are the radii of the outer and inner surfaces of the spherical shell, respectively, and r is the geocentric distance from the computation point P to the center of the sphere.

The thickness of the spherical shell in this test is 1 km, so the radii of the inner and outer surfaces are $R_1 = 6370$ km and $R = 6371$ km, respectively; the constant density of the spherical shell is $\rho = 2670$ kg m^{-3}; and the gravitational constant is $G = 6.67428 \times 10^{-11}$ m^3 kg^{-1} s^{-2}. The computation point P is set on a sphere with a radius of $r_P = 6386$ km, at the position with longitude and latitude (45°2.5′E, 45°2.5′N) in our simulation test, to compare the results calculated by different order tesseroid formulas. We note that as a simulation test, the computation point can be selected anywhere on and outside the sphere. We select the distance of 6386 km because when the computation point is near the surface of the mass shell, the calculation error caused by the tesseroid formulas becomes relatively large (as discussed in Section 4.1), which may largely contaminate the comparison results. This is the near-surface singular problem as mentioned by different authors (*Klees, 1996*; *Klees and Lehmann, 1998*; *Gray et al., 2004*; *Khayat and Wilton, 2005*; *D'Urso, 2013*).

Thus, the true GP value at computation point P at 15 km height above the spherical shell generated by the spherical shell is $V_{\text{true}} = 14231.2705286321$ m^2 s^{-2} based on Eq. (16).

We divided the mass shell into different grids with various resolutions to calculate the potential generated by the spherical shell using tesseroid formulas. All relevant information is listed in Table 1, which also lists the total CPU-time costs in calculating the GP values of the spherical shell at the computation point P using different-order tesseroid formulas with different grid resolutions. Results are listed in Table 2, which shows the differences between the calculated and true values. Note that the order corresponds to which order the formula is referred to, namely, the zero-order formula provided by Eq. (13), the second-order formula provided by Eq. (14), and the fourth-order formula provided by Eq. (15). We note that all calculations in this paper are processed in a workstation with 32 CPUs in parallel, based on Mathematica software, in which the chosen significant digits are in double precision. The computation time cost depends on hardware. That means it depends on specific architecture of computer, its operational system and used compiler. Herein in this paper we just show the actual consuming time based on comparison of three different formulas (i.e. fourth-order, second-order, and zero-order formulas). As for the internal relations of the ratio of CPU time between three different formulas, it would approximately be fourth-order formula time cost/second-order formula time cost = 8 , second-order/zero-order = 8 and fourth-order/zero-order = 6. However, this approximation relation might be inapplicable at some lower resolutions (e.g., 5° × 5°, as listed in Table 1).

Corresponding to Table 1, Fig. 2 shows the total CPU-time cost for the calculations using the zero-order, second-order, and fourth-order formulas in $\log_{10}$ scale. The horizontal axis displays the grid resolution from 5° × 5° to 1.5′ × 1.5′, whereas the vertical axis shows the time cost in $\log_{10}$ scale. As shown by Fig. 2, the zero-order, second-order, and fourth-order values are described by three different curves, and as a whole, the trends of the three curves are approximately the same: the higher the grid resolution is, the more

Table 1. Time cost of different resolution grids and order models of tesseroid formulas (values in s).

Grid Resolution	Number of Grid Elements	Zero-Order		Second-Order		Fourth-Order		CPU Ratio		
		Total CPU Time	$10^6 \times$ CPU Time per Tesseroid	Total CPU Time	$10^6 \times$ CPU Time per Tesseroid	Total CPU Time	$10^6 \times$ CPU Time per Tesseroid	Fourth Order /Second Order	Second Order /Second Order	Fourth Order /Zero Order
1.5′×1.5′	103680000	72.8	0.7	558.1	5.4	4905.4	47.3	8.8	7.7	67.4
5′×5′	9331200	8.4	0.9	55.9	6.0	432.1	46.4	7.7	6.7	51.6
15′×15′	1036800	2.7	2.6	22.6	21.8	181.3	174.8	8.0	8.5	68.1
30′×30′	259200	0.6	2.4	5.9	22.6	40.9	158.0	7.0	9.5	66.5
1°×1°	64800	0.2	3.8	1.6	25.1	12.8	196.8	7.8	6.7	52.5
5°×5°	2592	0.04	15.4	0.06	23.1	0.2	77.2	3.3	1.5	5.0

Table 2. Comparison of the calculated values and the true value $V_{\text{true}} = 14231.2705286321\ \text{m}^2\ \text{s}^{-2}$ for the computation point with $r_P = 6386$ km.

Grid Resolution	Order	$V - V_{\text{true}}$ [$\text{m}^2\ \text{s}^{-2}$]
5′ × 5′	zero	–121.7
	second	–57.78
	fourth	–37.06
1′ × 1′	zero	–14.27
	second	–2.693
	fourth	–1.093
30′ × 30′	zero	–3.076
	second	5.459×10^{-1}
	fourth	4.899×10^{-1}
15′ × 15′	zero	-1.593×10^{-1}
	second	1.060×10^{-1}
	fourth	-2.237×10^{-2}
5′ × 5′	zero	1.224×10^{-3}
	second	-5.755×10^{-5}
	fourth	1.428×10^{-5}
1.5′ × 1.5′	zero	7.526×10^{-5}
	second	-5.639×10^{-11}
	fourth	-5.639×10^{-11}

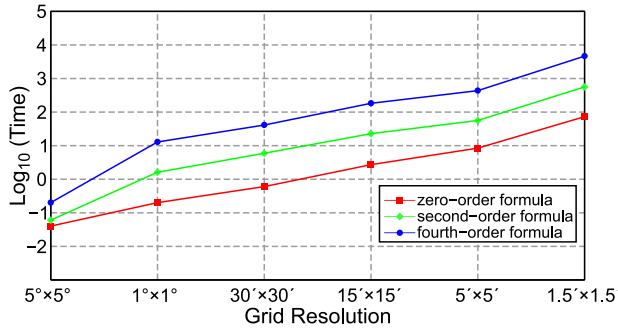

Fig. 2. Total CPU-time costs in the calculations using the zero-order, second-order, and fourth-order formulas.

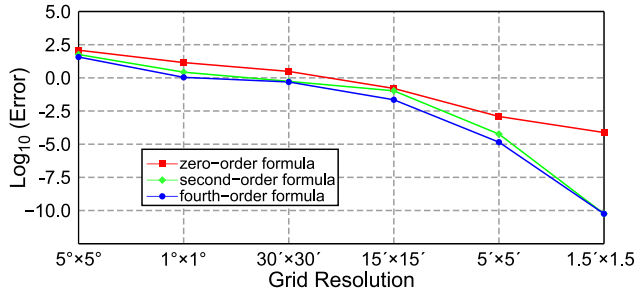

Fig. 3. Absolute differences between the true value and values calculated based on the zero-order, second-order and fourth-order formulas.

time it costs. As for the fourth-order formula, the time cost is highest in the three different curves at each grid resolution, which agrees well with theoretical equation derivation. And the time cost is less than 1000 s for the grid resolution larger than $5' \times 5'$ in the fourth-order formula, whereas the time cost for the grid resolution $1.5' \times 1.5'$ could substantially be as large as 4905.4 s.

Figure 3 shows the differences between the calculated and corresponding true values in $\log_{10}$ scale. The horizontal axis is the grid resolution from $5 \times 5°$ to $1.5' \times 1.5'$, whereas the vertical axis is the absolute error of the GP value (in $m^2\ s^{-2}$) in $\log_{10}$ scale, namely, the absolute difference between the calculated and corresponding true values in $\log_{10}$ scale. The zero-order, second-order, and fourth-order values are denoted by three different curves, as shown by Fig. 3. As the grid resolution becomes smaller, the absolute differences also become smaller. After the grid resolution reaches $1.5' \times 1.5'$, the magnitudes of second-order and fourth-order formulas are in the level of 10^{-11}, and the magnitude of zero-order formula is in the level of 10^{-5}.

The numerical results show that the fourth-order tesseroid formula with the grid resolution $1.5' \times 1.5'$ can reach the highest accuracy in computing the potential of the spherical shell. The computation time costs are also the largest. Thus, selecting the order

of the tesseroid formula with proper grid resolution should be considered for both the efficiency and precision. For instance, at this special point P, if an accuracy of about 2 mm with a grid resolution of $15' \times 15'$ is required, we can select the fourth-order tesseroid formula that can guarantee an accuracy of 2.2 mm (Table 2). However, if a higher precision is required, a higher grid resolution is also required under the assumption that the fourth-order tesseroid formula is applied. Figures 3 shows that the fourth-order formula is correct, because it improves all grid-resolutions.

Herein, compared to the spherical shell with thickness 1 km, the spherical shell with thickness 8 km as a worst-case scenario for high mountainous areas is chosen for simulations of the elevated terrain, where the grid resolution is set as $5'$ and other conditions hold the same as mentioned above. The computation time costs of different order tesseroid formulas by comparing the spherical shell with thickness 8 km with that with thickness 1 km are nearly the same. However, the magnitudes of absolute errors of different order tesseroid formulas in the case of thickness 8 km can reach as 5.614×10^{-3} m^2 s^{-2} for zero-order tesseroid, 1.717×10^{-4} m^2 s^{-2} for second-order tesseroid, and 1.030×10^{-4} m^2 s^{-2} for fourth-order tesseroid, which are different from the corresponding results in the case of the thickness 1 km as 1.224×10^{-3} m^2 s^{-2} for zero-order tesseroid, 5.755×10^{-5} m^2 s^{-2} for second-order tesseroid, and 1.428×10^{-6} m^2 s^{-2} for fourth-order tesseroid. In summary, it means that the shell thickness (or the elevated terrain) may influence the computation precision but not time cost, because the absolute errors are much larger for thicker shell, but they are still acceptable in related application of GP calculation.

4. NUMERICAL TESTS FOR VERY-NEAR-ZONE AND POLAR-REGION CALCULATION PROBLEMS

4.1. Influence of the vertical distance between the computation point and the center of the sphere

The tesseroid formula (e.g., second-order tesseroid formula) at the very-near-area of the computation point should be used carefully. *Heck and Seitz (2007)* and *Grombein et al. (2013)* pointed out that the distance between the geometric center of the tesseroid and the computation point affects the calculation accuracy of the GP, where this corresponds to space borne applications. This section further demonstrates that the distance of the computation point from the sphere center affects the accuracy of the calculated GP.

It will be more precise if the calculation with higher resolution could be executed. However, the higher resolution (i.e. $3''$) is used, the more time the calculation will cost (see the log scale time costs in the calculations as shown by Fig. 2). Here in this study we only apply the resolution of $15' \times 15'$ and $5' \times 5'$ in terms of computation time cost. We used the fourth-order Eq. (15) with the shell divided by $15' \times 15'$ and $5' \times 5'$ grid to critically test the influence of the distance from the computation point to the sphere center. We modified the distance between the sphere center and computation point P from $R = 6371$ km (on the outer surface of the spherical shell) to 6401 km at an interval of 0.15 km. *Heck and Seitz (2007)* stated that there exist evident errors as large as 10^{-3} m^2 s^{-2} in the case of grid of $5' \times 5'$ resolution for P at the pole and thickness of 1 km

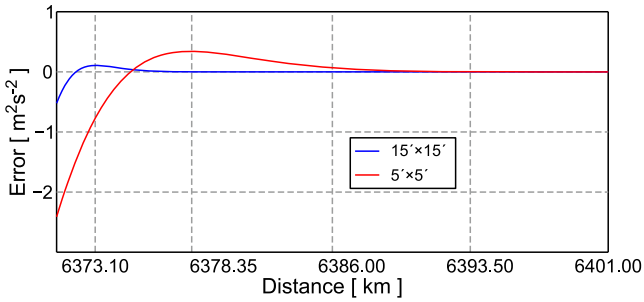

Fig. 4. Gravitational potential differences between the values computed using the fourth-order formula Eq. (15) and true value at the computation point above the equator that runs from 6371 km to 6401 km outside the shell. The shell is divided by 15′ × 15′ and 5′ × 5′ grids.

near the north pole by providing the numerical results with the analytical solution of a spherical zonal band when the computation point is on top of the surface. They considered that large errors were caused by the short distance between the mass element and the computation point, as well as the truncation error of the Taylor expansion. At this point, we presented the errors caused by the fourth-order tesseroid formula when the computation point P moves from the surface with radius of 6371 km to a distance of 6401 km away from the center of the shell. Without loss of generality for the optimal choice of the position of the computation point, the longitude and latitude of the computation point P are selected as (0°E, 0°N).

Figure 4 shows the error variation trends among the calculated values using the fourth-order Eq. (15) with different grid divisions (15′ × 15′ and 5′ × 5′, respectively) and the corresponding true values. The horizontal axis denotes the geocentric distance r_P of the computation point P. From Fig. 4 we can see that, on the whole, the trends of both curves are similar; though the error of the latter one is smaller than that of the former one. Specifically, with the resolution of 15′ × 15′, the error monotonously changes from -2.41 m^2 s^{-2} to the maximum value of 0.34 m^2 s^{-2} when r_P changes from 6371 km to 6378.35 km, and monotonously decreases from 0.34 m^2 s^{-2} to -1.6622×10^{-3} m^2 s^{-2} when r_P changes from 6378.35 km to 6401 km, and tends to zero as r_P approaches infinity; whereas with the resolution of 5′ × 5′, the error monotonously changes from -0.52 m^2 s^{-2} to the maximum value of 0.11 m^2 s^{-2} when r_P changes from 6371 km to 6373.1 km, and decreases from 0.11 m^2 s^{-2} to -1.0841×10^{-9} m^2 s^{-2} when r_P changes from 6373.1 km to 6401 km, and tends to zero as r_P approaches infinity.

Thus, the errors caused by the fourth-order formula are quite large at the very near-area of the computation point. This very near-zone problem will be discussed in Section 4.3.

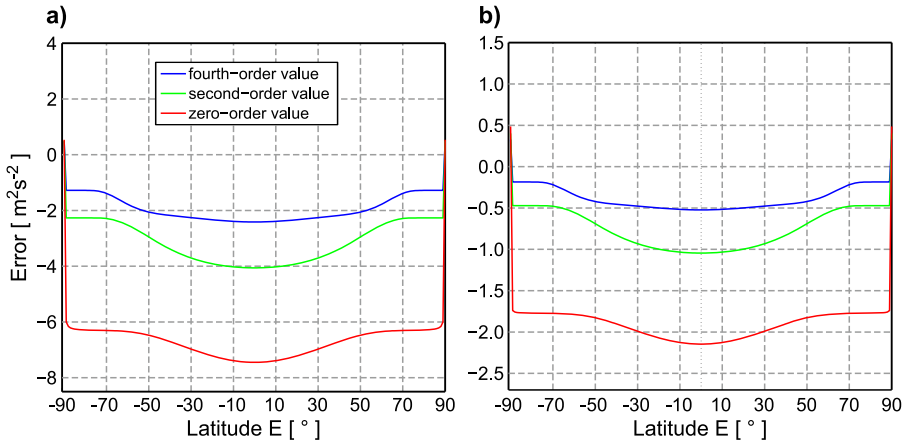

Fig. 5. Influence of the latitude of the computation point P in calculating the gravitational potential of the spherical shell using the zero-order, second-order, and fourth-order formulas. The shell divided by **a)** $15' \times 15'$ grid, and, **b)** $5' \times 5'$ grid. Note that the figures show the differences between the calculated values using one of the different-order tesseroid formulas and corresponding true values.

4.2. Influence of the latitude of the computation point P on the potential

In this numerical test we set the coordinates of the computation point $P(r, \varphi, \lambda)$ to $r_P = 6371$ km and $\lambda_P = 0$ as constants, and φ_P changes from the south pole (at –90°) through the equator to the north pole (90°, see Fig. 5). The values are calculated for every 5° interval change in latitude φ.

Considering computation time cost of higher resolution (i.e. 1″ or 3″), which is the same as described in Section 4.1, here we only deal with the case of resolution $15' \times 15'$ and $5' \times 5'$. For higher resolution, further investigations are needed. Hence, the shell is divided by $15' \times 15'$ (Fig. 5a) and $5' \times 5'$ grids (Fig. 5b) in our calculations.

The results for the computation points at the south and north poles are extremely anomalous because of the jumping errors which are caused by polar singularity. According to *Grombein et al. (2013)*, using the tesseroid method in a satellite orbit of 260-km height, results for elements of the Marussi tensor (second derivatives of GP) are in large errors when the computation point P is at the north pole, where the critical limit is at $\varphi > 85°$. In the present study, we find that the tesseroid formulas cannot be directly applied to the polar regions due to poor fitting of the divided grids and the tesseroidal figuration. Thus, the GP of computation point at the polar regions cannot be properly modeled by the tesseroid formula and should be considered by other more accurate formulas (Section 4.3).

4.3. Solution of the very near-zone problem using a new combination method

4.3.1. New combination method

Based on *Martinec (1998)* and *Heck and Seitz (2007)*, when the integration of r' is analytically evaluated from Eq. (1), the GP of the surface integral can be written as follows:

$$V(r,\varphi,\lambda)=\frac{1}{2}G\rho\int_{\lambda_1}^{\lambda_2}\int_{\varphi_1}^{\varphi_2}\cos\varphi'\Big[l\left(r'+3\cos\psi\right)+r^2\left(3\cos^2\psi-1\right)\ln\left(l+r'-r\cos\psi\right)\Big]_{r'=r_1}^{r'=r_2}d\varphi'\,d\lambda'. \tag{17}$$

This integral is still of elliptic type and cannot be integrated analytically. As for comparison in the next numerical tests, Eq. (17) is evaluated numerically for it still has to be discretized and it will generate numerical errors. Therefore, the numerical precision of Eq. (17) is setting as 10^{-25} m^2 s^{-2} with the built-in function of Mathematica software, which means within the computer accuracy range, this formula is numerically precise for sufficiently satisfying the actually required calculation comparison precision. Nevertheless, in the sequel Eq. (17) is referred to as "precise numerical formula". Note that herein the Gauss-Legendre Quadrature (GLQ) numerical method (*Ku, 1977*; *von Frese et al., 1981*; *Asgharzadeh et al., 2007*; *Hirt et al., 2011*; *Roussel et al., 2015*) is recommended to apply in further investigations.

Without loss of generality, in this study the computation point P is simply placed at the crossing point of the prime meridian and equator on the spherical surface. In particular, the spherical coordinates of the computation point P are $r_P = 6371$ km, $\lambda_P = 0$ and $\varphi_P = 0$. Given the spherical symmetry, the results are the same for any computation point on the equator, where it should be noted that the computation point can be located above the corner, the edge of a tesseroid, or above center of cell. And therefore the results can slightly differ especially for the input of the tesseroids from the nearest neighborhood.

As a preliminary comparison with a grid resolution of $5' \times 5'$, the potentials of the shell were respectively calculated using only the fourth-order tesseroid formula (15), or second-order formula (14), or zero-order formula (13). The results are listed in Table 3a, Case A, which show that the accuracy is insufficient. The absolute error caused by the fourth-order tesseroid formula can reach 0.52299 m^2 s^{-2} (which is equivalent to about 5 cm in height), whereas the absolute errors caused by the second-order and zero-order are both larger than 1.0 m^2 s^{-2} (which is equivalent to 10 cm in height).

The results using the conventional combination method, i.e., combination of the prism model (in the very near region, e.g., spherical distance $\psi \leq 1°$ with the $5' \times 5'$ grid, and with the resolution of the grid being smaller - the spherical distance can also be lessened) and different tesseroid formulas (in other regions), are listed in Table 3a, Case B. The accuracy is significantly improved but still insufficient for high-precision applications. Note that the prism method (*Nagy et al., 2000, 2002*) has a rigorous and closed expression and can be solved analytically in the domain both inside and outside the prism (*Han and*

Table 3a. Three cases. **A)** Gravitational potential (GP) comparison between the calculated values based on different calculation formulas (e.g., fourth-order, second-order and zero-order) and true value (14264.776895 $m^2\ s^{-2}$) of point P at the equator on the sphere surface $r_P = 6371$ km, with a $5' \times 5'$ grid; **B)** GP comparison between the calculated values by different conventional combination methods (prism formula ($\psi \leq 1°$) + different order tesseroid formulas ($\psi > 1°$)) and true value of point P on the equator of the sphere surface $r_P = 6371$ km, with a $5' \times 5'$ grid; **C)** GP comparison between the calculated values by the new combination method (precise numerical formula ($\psi \leq 1°$) + different order tesseroid formulas ($\psi > 1°$)) and true value of point P on the equator of the sphere surface $r_P = 6371$ km, with a $5' \times 5'$ grid.

Case	Combination Method	Error [$m^2\ s^{-2}$]	Time Cost [s]
A	Using the fourth-order formula (15)	–0.5230	422.02
	Using the second-order formula (14)	–1.0450	54.20
	Using the zero-order formula (13)	–2.1463	8.14
B	Prism formula +fourth-order tesseroid	0.0089145	15044.59
	Prism formula +second-order tesseroid	0.0089092	14680.41
	Prism formula +zero-order tesseroid	–0.022247	14630.55
C	Precise numerical formula +fourth-order tesseroid	-2.9959×10^{-9}	926.20
	Precise numerical formula +second-order tesseroid	-5.3355×10^{-6}	562.02
	Precise numerical formula +zero-order tesseroid	–0.0312	512.17

Shen, 2010), the computation time cost of the prism method could be reduced to a manageable level by using the two-grid approach with super-computers, with one high-resolution grid in the vicinity of the computation points and a low-resolution grid (e.g., reduced by factor 5 in resolution, corresponding to a reduction by factor 25 in terms of mass elements to be considered) in the far-zone (*Forsberg, 1984*; *Kuhn et al., 2009*). Although the conventional combination method is widely used in local geoid determination (e.g., *Tsoulis et al., 2009*; *Shen and Han, 2013*) or global geoid determination (*Shen and Han, 2014, 2016*), the results listed in Table 3a, Case B, show that the accuracy is limited. From these results as listed in Table 3a case B, we can conclude that the approximation error of the prisms is 0.0089 $m^2\ s^{-2}$.

Hence, we propose a new combination to precisely determine the potential. This combination includes the precise numerical formula (in the very near region, e.g., spherical distance $\psi \leq 1°$) and different tesseroid formulas (in other regions). The results are listed in Table 3a, Case C. We find that the accuracy is largely improved (achieving $10^{-6}\ m^2\ s^{-2}$ level) and satisfies the high-precision application requirements when using the combination of the precise numerical formula and second-order tesseroid model. The accuracy can even reach $10^{-9}\ m^2\ s^{-2}$ for the combination of the precise numerical formula and fourth-order tesseroid model, which can satisfy the ultra-high precision requirement in global-scale applications.

Table 3a clearly shows that the problem of the very-near-zone of the computation point can be solved by the new combination method, namely the combination of the precise numerical formula Eq. (17) and different-order tesseroid formulas.

Table 3b. Test for selection of the boundary between the near zone and transition region. The shell is divided by a 5′ × 5′ grid for precise numerical formula (spherical distance $\psi \leq 1°$) +fourth-order tesseroid (1° to α) + second-order tesseroid (outside α).

Area Range α [°]	Error [$m^2\ s^{-2}$]	Time Cost [s]
5	-4.5740×10^{-8}	576.60
10	-8.3000×10^{-9}	580.23
15	-4.5475×10^{-9}	581.41
20	-3.6416×10^{-9}	587.64
30	-3.1796×10^{-9}	597.84
60	-3.0122×10^{-9}	657.06
90	-3.0032×10^{-9}	759.09

Table 3c. Test for selection of the boundary between transition region and far zones, where the second-order and zero-order tesseroid formulas are applied. The shell is divided by a 5′ × 5′ grid for precise numerical formula (spherical distance $\psi \leq 1°$) +fourth-order tesseroid (1°–15°) + second-order tesseroid (15° to β) + zero-order tesseroid (outside β)

Area Range β [°]	Error [$m^2\ s^{-2}$]	Time Cost [s]
30	-2.6631×10^{-4}	536.86
40	-2.1813×10^{-5}	538.88
50	1.1708×10^{-4}	541.31
60	2.0400×10^{-4}	544.77
90	3.3171×10^{-4}	558.85

4.3.2. Best match in selecting different-order tesseroid formulas for different areas

We conducted different numerical tests to determine which combination type can obtain the "optimal results" or "best match" that considers the efficiency and precision.

The spherical distance ($\psi \leq 1°$) of very-near-zone around the computation point was calculated using the precise numerical formula (17). Different integration zones with a max spherical distance α of the fourth-order and second-order tesseroid formulas with a 5′ ×5′ grid were then selected to calculate the potential. The results are listed in Table 3b. We see from Table 3b that the accuracy gradually increases to $10^{-9}\ m^2\ s^{-2}$ with the increase in α until 10°. The time cost also gradually increases. The time cost for $\alpha = 15°$ is approximately 1 s more than that for $\alpha = 10°$, whereas the accuracy improves by nearly 50% from -8.3000×10^{-9} to $-4.5475 \times 10^{-9}\ m^2\ s^{-2}$. However, the time cost for $\alpha = 20°$ is approximately 5 s more than that for $\alpha = 15°$, but the accuracy improves by only 25%. Considering both the accuracy requirement and economical efficiency, we selected $\alpha = 15°$ as the boundary between the near zone and transition region. Thus, if we

use the fourth-order tesseroid model in the near zone ($1° \le \alpha \le 15°$), and second-order tesseroid model in the transition region and far zone ($\alpha \ge 15°$), the accuracy can reach 4.5×10^{-9} m^2 s^{-2} (with the time cost of 581.41 s).

In Table 3c, it might be assumed that the errors become smaller with increase of β because more tesseroids are evaluated with second-order instead of zero-order, but actually it does not show this is true. As for the reason, we may consider that it is simply due to the fact that zero-order tesseroid formula and second-order tesseroid formula have a zero-crossing between $40° \le \beta \le 50°$. Both masses produce the same potential (by accidence) for a special β. Further investigations about the zero-crossing problem will be implemented in the future.

If we use the methods as listed in Table 3c, the calculation precision cannot reach 10^{-9} m^2 s^{-2} level. However, if we use the methods as listed in Table 3b the accuracy level 10^{-9} m^2 s^{-2} can be reached. That means the zero-order formula cannot be used at the ultra-high accuracy (i.e. 10^{-9} m^2 s^{-2} level) requirement. And the zero-order tesseroid formula, which is frequently recommended to be applied at the very far-zone of the computation point (e.g., *Heck and Seitz, 2007*; *Tsoulis et al., 2009*; *Shen and Han, 2013, 2014, 2016*; *Tsoulis et al., 2013*), should be not recommended to be applied globally when the ultra-high accuracy is required due to the fact that the contribution of zero-order tesseroid formula in far-zone is also obvious. Hence, in this case, we should use the second-order tesseroid formula in the far area (including very far-area). Therefore, based on the calculations (Tables 3b and 3c), if the accuracy requirement is at the level of 10^{-5} m^2 s^{-2}, we can use the precise numerical formula, fourth-order tesseroid, second-order tesseroid, and zero-order tesseroid formulas in the ranges of 0°–1°, 1°–15°, 15°–40°, and other zones, respectively. However, if the accuracy requirement is higher, such as 10^{-9} m^2 s^{-2} (see Table 3b), we should give up the zero-order tesseroid formula and just use the precise numerical formula in the very near region (spherical distance $\psi \le 1°$), fourth-order tesseroid formula in the near region (1°–15°), and second-order tesseroid formula in the transition and far zones (region outside 15°).

4.4. Calculation solution in the polar region using a new combination method

Here the computation point P is located at the north pole. Other conditions are similar to those presented in Section 4.3. The contributions to the potential of a spherical shell are calculated using the fourth-order tesseroid formula (15), the second-order tesseroid formula (14), and the zero-order tesseroid formula (13). Results are listed in Table 4a, Case A. Figure 5 shows that the value error of the north polar point is a jumping point and the accuracy is insufficient. The results computed by the conventional combination method, i.e., the combination of the prism model (in the very near region, i.e., spherical distance $\psi \le 1°$) and different tesseroid formulas (in other regions), are listed in Table 4a, Case B. The results are poor because the prism model does not properly consider the Earth's curvature and coverage of the meridian at the polar region. However, significantly improved results are obtained using the new combination, i.e., a combination of the precise numerical formula (in the very near region, i.e., spherical distance $\psi \le 1°$) and different tesseroid formulas (in other regions), which are listed in Table 4a, Case C. The

Table 4a. The same as in Table 3a, but for the north pole.

Case	Combination Method	Error [$m^2\ s^{-2}$]	Time Cost [s]
A	Using the fourth-order formula (15)	0.32849	448.94
	Using the second-order formula (14)	0.40241	59.04
	Using the zero-order formula (13)	0.48608	8.57
B	Prism formula +fourth-order tesseroid	15.219410	15078.00
	Prism formula +second-order tesseroid	15.219410	14681.89
	Prism formula +zero-order tesseroid	15.220127	14630.62
C	Precise numerical formula +fourth-order tesseroid	2.4193×10^{-10}	457.34
	Precise numerical formula +second-order tesseroid	2.4162×10^{-7}	61.23
	Precise numerical formula +zero-order tesseroid	7.1728×10^{-4}	9.95

accuracy can reach 7.1728×10^{-4} $m^2\ s^{-2}$ at 10 s using the new combination method (i.e., combination of the precise numerical formula and zero-order tesseroid model), which can satisfy the general application in the common use for the terrain effect. The accuracy is largely improved to 10^{-7} $m^2\ s^{-2}$ and the time cost is above 1 min using the combination of the precise numerical formula and second-order tesseroid model. This method satisfies the general high-precision application requirements both for high precision and relatively high efficiency. However, if ultra-high precision is required at the polar point, it can be calculated using the combination of the precise numerical formula and fourth-order tesseroid model, which can achieve an accuracy of 10^{-10} $m^2\ s^{-2}$.

Similar to Section 4.3.2, the best match in selecting different-order tesseroid formulas for different areas with respect to the north pole, as shown in Tables 4b,c. Similar to selecting the boundary between the transition region and far zone in Section 4.3.2, the results are presented in Table 4b, which shows that the accuracy steadily increases and remains stable at 10^{-10} $m^2\ s^{-2}$ with the increase in α from 5° to 90°. The time cost also increases steadily. With the increase in α from 5° to 10° , the accuracy significantly increases from 2.1719×10^{-9} to 4.7839×10^{-10} $m^2\ s^{-2}$, whereas the time cost is approximately 10 s more. The time cost for $\alpha = 15°$ is approximately 10 s more than that for $\alpha = 10°$, whereas the accuracy is only improved by 35%. Considering both for the accuracy requirement and economical efficiency, we select 10° as the boundary between the transition region and far zone, which is slightly different from the condition on the equator.

If the accuracy requirement is at the level of 10^{-4} $m^2\ s^{-2}$ (Table 4c), which can satisfy general applications, $\beta = 30°$ is recommended. If the accuracy requirement is at the level of 10^{-5} $m^2\ s^{-2}$, we can simply use the precise numerical formula, fourth-order tesseroid, and the second-order tesseroid formulas in the ranges of 0°–1°, 1°–10°, and the rest zones.

Table 4b. The same as in Table 3b, but for the north pole.

Area Range α [°]	Error [$m^2\ s^{-2}$]	Time Cost [s]
5	2.1719×10^{-9}	72.15
10	4.7839×10^{-10}	82.68
15	3.0923×10^{-10}	94.15
30	2.4920×10^{-10}	124.07
60	2.4193×10^{-10}	190.01
90	2.4011×10^{-10}	253.81

Table 4c. Test for selection of the boundary between transition region and far zones, where the second-order and zero-order tesseroid formulas are applied to the north pole, with a $5' \times 5'$ grid for precise numerical formula (spherical distance $\psi \leq 1°$) +fourth-order tesseroid (1°–10°) + second-order tesseroid (10° to β) + zero-order tesseroid (outside β)

Area Range β [°]	Error [$m^2\ s^{-2}$]	Time Cost [s]
30	2.2533×10^{-4}	41.69
60	1.5534×10^{-4}	50.00
90	9.0368×10^{-5}	58.54

4.5. Results at different latitudes using the new combination method

The new combination method is applied to the situation where the computation point is at different latitudes from 30° to 60° on the spherical surface. Similar computing strategies that calculate the GP of the shell using different models are adopted. The following calculation schemes are presented:

1. If the computation point is in the low-latitude zone (e.g., 30°, 40°, and 45°(A)), we use the precise numerical formula, fourth-order tesseroid, second-order tesseroid, and zero-order tesseroid formula in the ranges of 0°–1°, 1°–15°, 15°–40°, and the rest zones, respectively.
2. If the computation point is in the high-latitude zone (e.g., 45°(B), 50°, and 60°), we use the precise numerical formula, fourth-order tesseroid, second-order tesseroid, and zero-order tesseroid formula in the ranges of 0°–1°, 1°–10°, 10°–30°, and the rest zones, respectively.

The relevant results are listed in Table 5 at low accuracy. Table 5 at low accuracy shows that the accuracy of all of the calculated entities can reach $10^{-4}\ m^2\ s^{-2}$, which is consistent with the results in Tables 3e and 4e. The second calculation scheme 45°(B) is better than the first one 45°(A) for latitude 45°, where the time cost is less and the accuracy is higher. Thus, latitude 45° should be categorized under the high-latitude zone.

Table 5. Gravitational potential and time costs at different accuracy (low and high) and different latitudes using the new combination method with a 5′ × 5′ grid. A and B correspond to different calculation schemes (see text for details).

Accuracy	Latitude [°]	Error [$m^2\ s^{-2}$]	Time Cost [s]
Low	30	1.5797×10^{-4}	44.59
	40	3.2330×10^{-4}	53.09
	45 (A)	4.3696×10^{-4}	44.74
	45 (B)	2.3403×10^{-4}	36.71
	50	3.8815×10^{-4}	46.40
	60	8.2916×10^{-4}	36.25
High	30	6.8449×10^{-9}	105.94
	40	-3.4051×10^{-9}	135.05
	45	-8.1127×10^{-10}	102.66
	50	-9.7589×10^{-9}	176.49
	60	-1.1829×10^{-8}	97.34

However, if the accuracy requirement is higher than $10^{-5}\ m^2\ s^{-2}$, we should replace the zero-order tesseroid formula and use the second-order tesseroid formula instead in the low-latitude zone outside 40° or high-latitude zone outside 30°. Thus, for the low-latitude zone, we use the precise formula, fourth-order tesseroid, and the second-order tesseroid formulas in the ranges of 0°–1°, 1°–15°, and the rest zones, respectively. However, for the high-latitude zone, we use the precise numerical formula, fourth-order tesseroid, and second-order tesseroid formulas in the ranges of 0°–1°, 1°–10°, and rest zones, respectively. The relevant results are listed in Table 5 at high accuracy.

5. CONCLUSIONS

Comparisons among true analytical value of a spherical shell and the corresponding values calculated by various combinations of the zero-order, second-order, fourth-order and precise numerical tesseroid formulas are performed based on numerical calculations. The results show that different combination models and their corresponding computation time costs should be carefully considered to achieve sufficiently accurate results using the tesseroid formulas in different orders and different grid resolutions. For a given grid resolution (e.g., 5′ × 5′ grid), if more accurate results are required, the tesseroid formulas in higher-order Taylor series expansions should be applied.

Although the prism model can be extensively applied for the gravity forward modeling in the Newton integral, it has a key weak point because the surface of the Earth is bent. In addition, the time consumption using the prism model is 10 times larger than that using the second-order tesseroid (cf. *Heck and Seitz, 2007*). The advantages of using the second-order tesseroid to model the GP considering the numerical efficiency and accuracy compared with using the prism method have been discussed in several studies (cf. *Heck and Seitz, 2007*; *Wild-Pfeiffer, 2008*; *Grombein et al., 2013*).

This study re-investigated the very near-zone problem at the equator and north polar points using a new combination method of the precise numerical formula and different-order tesseroid formulas. Compared to different types of combination methods (i.e., prism formula and different-order tesseroid formulas), the combination approach proposed in this study can achieve high precision and efficiency in computing the GP. Thus, the new combination method has advantages especially in calculating a global potential of the shallow layer density distribution, for instance, for the purpose of a global geoid determination (*Shen and Han, 2014, 2016*).

Note that because of the special settings used in the numerical examples, calculation schemes mentioned above are only valid for these settings. With different grid resolutions and the required precision, the area of very-near zone, near zone, transition zone and far area may be different; it depends on real situation. Nevertheless it might be used as reference for the actual calculations of the topographic potential for the area choices of very-near zone, near zone, transition zone and far area.

Based on this simulative study, we suggest the following calculation schemes for the computation point at the global scale as spherical approximation to calculate the GP with grid resolution $5' \times 5'$. If the computation point is on the equator or in the low-latitude zone, one may use a combination of the precise numerical formula, fourth-order tesseroid, second-order tesseroid, and zero-order tesseroid formulas in the ranges of 0°–1°, 1°–15°, 15°–40°, and the rest zones, respectively. However, if the accuracy requirement is higher than 10^{-5} m^2 s^{-2}, one should set aside the zero-order tesseroid formula and use the second-order tesseroid formula instead in the range outside 40°.

If the computation point is in the polar region or high-latitude zone, one may use the precise numerical formula, fourth-order tesseroid, second-order tesseroid, and zero-order tesseroid formulas in the ranges of 0°–1°, 1°–10°, 10°–30°, and rest zones, respectively. Similarly, if the accuracy requirement is higher than 10^{-5} m^2 s^{-2}, one should set aside the zero-order tesseroid formula and use the second-order tesseroid formula instead in the range outside 30°.

APPENDIX A
COEFFICIENTS OF THE ZERO-ORDER, SECOND-ORDER AND FOURTH-ORDER TESSEROID FORMULAS

Here the coefficients K_{ijk}, used in Eqs (13)–(15), are derived. We note that these expressions contain the coordinates of $P(r, \varphi, \lambda)$ and $Q_0(r_0, \varphi_0, \lambda_0)$.

$$K_{000} = \frac{r_0^2 \cos\varphi_0}{l_0} \,, \tag{A-1}$$

$$K_{200} = \frac{3r_0^2 \cos\varphi_0 \; B^2}{l_0^5} - \frac{r_0^2 \cos\varphi_0 + 4r_0 \cos\varphi_0 \; B}{l_0^3} + \frac{2\cos\varphi_0}{l_0} \,, \tag{A-2}$$

$$K_{020} = \frac{3r^2 r_0^4 \cos\varphi_0 \; A^2}{l_0^5} - \frac{r \, r_0^3 \left(2\sin\varphi_0 \; A + \cos\varphi_0 \; \cos\psi_0\right)}{l_0^3} - \frac{r_0^2 \cos\varphi_0}{l_0} \,, \tag{A-3}$$

$$K_{002} = \frac{3r^2 r_0^4 \sin^2(\lambda-\lambda_0)\cos^2\varphi\cos^3\varphi_0}{l_0^5} - \frac{r\, r_0^3 \cos\varphi\cos^2\varphi_0\cos(\lambda-\lambda_0)}{l_0^3}, \quad \text{(A-4)}$$

$$\begin{aligned} K_{400} = {} & \frac{105 r_0^2 \cos\varphi_0\, B^4}{l_0^9} - \frac{30 r_0 \cos\varphi_0\, B^2(3r_0+4B)}{l_0^7} \\ & + \frac{9\cos\varphi_0\left(r_0^2+8r_0B+4B^2\right)}{l_0^5} - \frac{12\cos\varphi_0}{l_0^3}, \end{aligned} \quad \text{(A-5)}$$

$$\begin{aligned} K_{040} = {} & \frac{105 r^4 r_0^6 A^4\cos\varphi_0}{l_0^9} - \frac{30 r^3 r_0^5 A^2(3\cos\varphi_0\cos\psi_0+2A\sin\varphi_0)}{l_0^7} \\ & + \frac{3r^2 r_0^4\left(12A\sin\varphi_0\cos\psi_0 - 6A^2\cos\varphi_0 + 3\cos\varphi_0\cos^2\psi_0 - 4A^2\cos\varphi_0\right)}{l_0^5} \\ & + \frac{r\, r_0^3(8A\sin\varphi_0+7\cos\varphi_0\cos\psi_0)}{l_0^3} + \frac{r_0^2\cos\varphi_0}{l_0}, \end{aligned} \quad \text{(A-6)}$$

$$\begin{aligned} K_{004} = {} & \frac{105 r^4 r_0^6 \cos^4\varphi\cos^5\varphi_0\sin^4(\lambda-\lambda_0)}{l_0^9} \\ & - \frac{90 r^3 r_0^5 \cos^3\varphi\cos^4\varphi_0\sin^2(\lambda-\lambda_0)\cos(\lambda-\lambda_0)}{l_0^7} \\ & - \frac{3r^2 r_0^4\cos^2\varphi\cos^3\varphi_0\left(4-7\cos^2(\lambda-\lambda_0)\right)}{l_0^5} + \frac{r\, r_0^3\cos\varphi\cos^2\varphi_0\cos(\lambda-\lambda_0)}{l_0^3}, \end{aligned} \quad \text{(A-7)}$$

$$\begin{aligned} K_{220} = {} & \frac{105 r^2 r_0^4 A^2 B^2\cos\varphi_0}{l_0^9} \\ & - \frac{15 r\, r_0^3\left[\cos\varphi_0\left(B^2\cos\psi_0 + A^2 r\, r_0\right) + AB\left(8Ar\cos\varphi_0 + B\sin\varphi_0\right)\right]}{l_0^7} \\ & + \frac{3r_0^2\left[\cos\varphi_0\left(12A^2r^2 - B^2\right) + rA\sin\varphi_0(r_0+10B) + r(6B+r_0)\cos\varphi_0\cos\psi_0\right]}{l_0^5} \\ & + \frac{r_0^2\cos\varphi_0 - 12Ar\, r_0\sin\varphi_0 - 6r\, r_0\cos\varphi_0\cos\psi_0 + 4Br_0\cos\varphi_0}{l_0^3} - \frac{2\cos\varphi_0}{l_0}, \end{aligned} \quad \text{(A-8)}$$

$$
\begin{aligned}
K_{202} &= \frac{105 r^2 r_0^4 B^2 \cos^4\varphi \cos^3\varphi_0 \sin^2(\lambda-\lambda_0)}{l_0^9} \\
&- \frac{15 r\, r_0^3 \cos\varphi \cos^2\varphi_0 \left[B^2 \cos(\lambda-\lambda_0) + r(r_0+8B)\cos\varphi\cos\varphi_0 \sin^2(\lambda-\lambda_0)\right]}{l_0^7} \\
&+ \frac{3 r\, r_0^2 \cos\varphi \cos^2\varphi_0 \left[(r_0+6B)\cos(\lambda-\lambda_0) + 12 r\cos\varphi\cos\varphi_0 \sin^2(\lambda-\lambda_0)\right]}{l_0^5} \\
&- \frac{6 r\, r_0 \cos\varphi \cos^2\varphi_0 \cos(\lambda-\lambda_0)}{l_0^3},
\end{aligned}
\tag{A-9}
$$

$$
\begin{aligned}
K_{022} &= \frac{105 A^2 r^4 r_0^6 \cos^2\varphi \cos^3\varphi_0 \sin^2(\lambda-\lambda_0)}{l_0^9} \\
&- \frac{15 r^3 r_0^5 \cos\varphi \cos^2\varphi_0}{l_0^7} \\
&\times \left[\cos\varphi (6A\sin\varphi_0 + \cos\varphi_0 \cos\psi_0)\sin^2(\lambda-\lambda_0) + A^2 \cos(\lambda-\lambda_0)\right] \\
&+ \frac{3 r^2 r_0^4 \cos\varphi\cos\varphi_0}{l_0^5} \left[(4A\sin\varphi_0 + \cos\varphi_0\cos\psi_0)\cos(\lambda-\lambda_0) \right. \\
&\left. + 3(2-3\cos^2\varphi_0)\cos\varphi \sin^2(\lambda-\lambda_0)\right] \\
&+ \frac{2 r\, r_0^3 (2\cos^2\varphi_0 - 1)\cos\varphi\cos(\lambda-\lambda_0)}{l_0^3},
\end{aligned}
\tag{A-10}
$$

where

$$
l_0 = \sqrt{r^2 - 2 r_0 r \left(\cos(\lambda-\lambda_0)\cos\varphi\cos\varphi_0 + \sin\varphi\sin\varphi_0\right) + r^2}
$$

is the Euclidean distance between P and Q_0, and

$$
\cos\psi_0 = \sin\varphi\sin\varphi_0 + \cos(\lambda-\lambda_0)\cos\varphi\cos\varphi_0 \ ,
$$

$$
A = \cos\varphi_0 \sin\varphi - \cos(\lambda-\lambda_0)\cos\varphi\sin\varphi_0 \ , \qquad B = r_0 - r\cos\psi_0 \ .
$$

Acknowledgements: We are grateful to two anonymous reviewers, as well as the Editor-in-Chief, for their valuable comments and suggestions, which greatly improved the manuscript. This study is supported by National 973 Project China (grants Nos 2013CB733301, 2013CB733305), and NSFC (grant Nos. 41174011, 41210006, 41021061, 40974015).

References

Anderson E.G., 1976. *The Effect of Topography on Solutions of Stokes' Problem*. School of Surveying, University of New South Wales, Kensington, NSW, Australia.

Asgharzadeh M.F., Von Frese R.R.B., Kim H.R., Leftwich T.E. and Kim J.W., 2007. Spherical prism gravity effects by Gauss-Legendre quadrature integration. *Geophys. J. Int.*, **169**, 1–11.

Bassin C., Laske G. and Masters G., 2000. The current limits of resolution for surface wave tomography in North America. *EOS Trans. AGU*, **81**, F897.

Chaves C.A.M. and Ussami N., 2013. Modeling 3-D density distribution in the mantle from inversion of geoid anomalies: Application to the Yellowstone Province. *J. Geophys. Res.*, **118**, 6328–6351.

Claessens S.J. and Hirt C., 2013. Ellipsoidal topographic potential: New solutions for spectral forward gravity modeling of topography with respect to a reference ellipsoid. *J. Geophys. Res.*, **118**, 5991–6002.

Deng X.L., Grombein T., Shen W.B., Heck B. and Seitz K., 2016. Corrections to "A comparison of the tesseroid, prism and point-mass approaches for mass reductions in gravity field modelling" (Heck and Seitz, 2007) and "Optimized formulas for the gravitational field of a tesseroid" (Grombein et al., 2013). *J. Geodesy*, **90**, 585–587.

D'Urso M.G., 2012. New expressions of the gravitational potential and its derivates for the prism. In: Sneeuw N., Novák P., Crespi M. and Sansò F. (Eds), *VII Hotine-Marussi International Symposium on Mathematical Geodesy*. International Association of Geodesy Symposia, **137**, 251–256. Springer-Verlag, Berlin, Germany.

D'Urso M.G., 2013. On the evaluation of the gravity effects of polyhedral bodies and a consistent treatment of related singularities. *J. Geodesy*, **87**, 239–252.

D'Urso M.G., 2014. Analytical computation of gravity effects for polyhedral bodies. *J. Geodesy*, **88**, 13–29.

Du J., Chen C., Lesur V., Lane R. and Wang H., 2015. Magnetic potential, vector and gradient tensor fields of a tesseroid in a geocentric spherical coordinate system. *Geophys. J. Int.*, **201**, 1977–2007.

Forsberg R., 1984. *A Study of Terrain Reductions, Density Anomalies and Geophysical Inversion Methods in Gravity Field Modelling*. Technical Report 355. Department of Geodetic Science and Surveying, The Ohio State University, Columbus, OH.

Gray L.J., Glaeser J.M. and Kaplan T., 2004. Direct evaluation of hypersingular Galerkin surface integrals. *SIAM J. Sci. Comput.*, **25**, 1534–1556.

Grombein T., Seitz K. and Heck B., 2013. Optimized formulas for the gravitational field of a tesseroid. *J. Geodesy*, **87**, 645–660.

Han J. and Shen W.B., 2010. Comparative study on two methods for calculating the gravitational potential of a prism. *Geospatial Inf. Sci.*, **13**, 60–64.

Heck B. and Seitz K., 2007. A comparison of the tesseroid, prism and point-mass approaches for mass reductions in gravity field modelling. *J. Geodesy*, **81**, 121–136.

Heiskanen W.A. and Moritz H., 1967. *Physical Geodesy*. Freeman, San Francisco, CA.

Hirt C., Claessens S., Fecher T., Kuhn M., Pail R. and Rexer M., 2013. New ultrahighresolution picture of Earth's gravity field. *Geophys. Res. Lett.*, **40**, 4279–4283.

Hirt C., Featherstone W.E. and Claessens S.J., 2011. On the accurate numerical evaluation of geodetic convolution integrals. *J. Geodesy*, **85**, 519–538.

Hirt C. and Kuhn M., 2014. Band-limited topographic mass distribution generates full-spectrum gravity field: Gravity forward modeling in the spectral and spatial domains revisited. *J. Geophys. Res.*, **119**, 3646–3661.

Hirt C., Marti U., Bürki B. and Featherstone W.E., 2010. Assessment of EGM2008 in Europe using accurate astrogeodetic vertical deflections and omission error estimates from SRTM/DTM2006.0 residual terrain model data. *J. Geophys. Res.*, **115**, B10404.

Hirt C. and Rexer M., 2015. Earth2014: 1 arc-min shape, topography, bedrock and ice-sheet models - available as gridded data and degree-10,800 spherical harmonics. *Int. J. Appl. Earth Obs. Geoinf.*, **39**, 103–112.

Jarvis A., Reuter H.I., Nelson A. and Guevara E., 2008. *Hole-Filled SRTM for the Globe, Version 4*. CGIAR-CSI SRTM 90m Database (http://srtm.csi.cgiar.org).

Jena B., Kurian P.J., Swain D., Tyagi A. and Ravindra R., 2012. Prediction of bathymetry from satellite altimeter based gravity in the Arabian Sea: Mapping of two unnamed deep seamounts. *Int. J. Appl. Earth Obs. Geoinf.*, **16**, 1–4.

Karcol R., 2011. Gravitational attraction and potential of spherical shell with radially dependent density. *Stud. Geophys. Geod.*, **55**, 21–34.

Khayat M.A. and Wilton D.R., 2005. Numerical evaluation of singular and near-singular potential integrals. *IEEE Trans. Antennas Propag.*, **53**, 3180–3190.

Kiamehr R. and Sjöberg L.E., 2005. Effect of the SRTM global DEM on the determination of a high-resolution geoid model: a case study in Iran. *J. Geodesy*, **79**, 540–551.

Kiamehr R., 2006. *Precise Gravimetric Geoid Model for Iran Based on GRACE and SRTM Data and the Least-Squares Modification of Stokes' Formula: with Some Geodynamic Interpretations*. Ph.D. Thesis. Royal Institute of Technology, Stockholm, Sweden.

Klees R., 1996. Numerical calculation of weakly singular surface integrals. *J. Geodesy*, **70**, 781–797.

Klees R. and Lehmann R., 1998. Calculation of strongly singular and hypersingular surface integrals. *J. Geodesy*, **72**, 530–546.

Ku C.C., 1977. A direct computation of gravity and magnetic anomalies caused by 2- and 3-dimensional bodies of arbitrary shape and arbitrary magnetic polarization by equivalent-point method and a simplified cubic spline. *Geophysics*, **42**, 610–622.

Kuhn M., 2003. Geoid determination with density hypotheses from isostatic models and geological information. *J. Geodesy*, **77**, 50–65.

Kuhn M., Featherstone W.E. and Kirby J.F., 2009. Complete spherical Bouguer gravity anomalies over Australia. *Aust. J. Earth Sci.*, **56**, 213-223.

Laske G., Masters G., Ma Z. and Pasyanos M., 2013. Update on CRUST1.0-A 1-degree global model of Earth's crust. *Geophys. Res. Abs.*, **15**, 2658.

Majumdar T.J. and Bhattacharyya R., 2014. High resolution satellite gravity over a part of the Sir Creek offshore on west northwest margin of the Indian subcontinent. *Indian J. Geo-Mar. Sci.*, **43**, 337–339.

Martinec Z., 1998. *Boundary Value Problems for Gravimetric Determination of a Precise Geoid*. Lecture Notes in Earth Sciences, **73**. Springer, Berlin, Heidelberg, New York.

Nagy D., Papp G. and Benedek J., 2000. The gravitational potential and its derivatives for the prism. *J. Geodesy*, **74**, 552–560.

Nagy D., Papp G., Benedek J., 2002. Corrections to "The gravitational potential and its derivatives for the prism". *J. Geodesy*, **76**, 475.

Reguzzoni M. and Sampietro D., 2015. GEMMA: An Earth crustal model based on GOCE satellite data. *Int. J. Appl. Earth Obs. Geoinf.*, **35**, 31–43.

Rexer M. and Hirt C., 2014. Comparison of free high resolution digital elevation data sets (ASTER GDEM2, SRTM v2.1/v4.1) and validation against accurate heights from the Australian National Gravity Database. *Aust. J. Earth Sci.*, **61**, 213–226.

Roussel C., Verdun J., Cali J. and Masson F., 2015. Complete gravity field of an ellipsoidal prism by Gauss-Legendre quadrature. *Geophys. J. Int.*, **203**, 2220–2236.

Shen W.B. and Han J., 2013. Improved geoid determination based on the shallow-layer method: A case study using EGM08 and CRUST2. 0 in the Xinjiang and Tibetan regions. *Terr. Atmos. Ocean Sci.*, **24**, 591–604.

Shen W.B. and Han J., 2014. The $5' \times 5'$ global geoid 2014 (GG2014) based on shallow layer method and its evaluation. *Geophys. Res. Abs.*, **16**, 12043.

Shen W.B. and Han J., 2016. The $5' \times 5'$global geoid model GGM2016. *Geophys. Res. Abs*., **18**, 7873.

Sjöberg L.E. and Bagherbandi M., 2011. A method of estimating the Moho density contrast with a tentative application of EGM08 and CRUST2.0. *Acta Geophys.*, **59**, 502–525.

Smith D.A., 2000. The gravitational attraction of any polygonally shaped vertical prism with inclined top and bottom faces. *J. Geodesy*, **74**, 414–420.

Tenzer R., Novák P., Gladkikh V. and Vajda P., 2012. Global crust-mantle density contrast estimated from EGM2008, DTM2008, CRUST2.0, and ICE-5G. *Pure Appl. Geophys*., **169**, 1663–1678.

Tsoulis D., 1999. *Analytical and Numerical Methods in Gravity Field Modelling of Ideal and Real Masses*. Ph.D. Thesis. Deutsche Geodätische Kommission, **C510**, München, Germany.

Tsoulis D., 2012. Analytical computation of the full gravity tensor of a homogeneous arbitrarily shaped polyhedral source using line integrals. *Geophysics*, **77**, F1–F11.

Tsoulis D., Novák P. and Kadlec M., 2009. Evaluation of precise terrain effects using high-resolution digital elevation models. *J. Geophys. Res.*, **114**, B02404.

Vaníček P., Novák P. and Martinec Z., 2001. Geoid, topography, and the Bouguer plate or shell. *J. Geodesy*, **75**, 210–215.

von Frese R.R.B., Hinze W.J., Braile L. and Luca A.J., 1981. Spherical Earth gravity and magnetic anomaly modeling by Gauss-Legendre quadrature integration. *J. Geophys.*, **49**, 234–242.

Wild-Pfeiffer F., 2008. A comparison of different mass elements for use in gravity gradiometry. *J. Geodesy*, **82**, 637–653.